

6-micron interaction length electro-optic modulation based on lithium niobate photonic crystal cavity

H. Lu,* B. Sadani, G. Ulliac, N. Courjal, C. Guyot, J. -M. Merolla, M. Collet, F. I. Baida, and M.-P. Bernal

Institut FEMTO-ST, UMR CNRS 6174, Université de Franche-Comté, 16 Route de Gray F-25030 Besançon Cedex, France

*huihui.lu@femto-st.fr

Abstract: We report on electro-optic modulation using a Lithium Niobate (LN) Photonic Crystal (PC) cavity structure. The compact device (6 μm in length) consists of a 2D photonic crystal cavity made on an Annealed Proton Exchange (APE) LN waveguide with vertical deposited electrodes. Experimental results show a tunability of 0.6 nm/V. This compact design opens a way towards micro and nano-scale tunable photonic devices with low driving electrical power.

© 2012 Optical Society of America

OCIS codes: (130.3730) Lithium niobate; (130.0250) Optoelectronics; (130.3990) Micro-optical devices; (250.4110) Modulators; (250.5300) Photonic integrated circuits.

References and links

1. E. Yablonovitch, "Inhibited spontaneous emission in solid-state physics and electronics," *Phys. Rev. Lett.* **58**(20), 2059–2062 (1987).
2. S. John, "Strong localization of photons in certain disordered dielectric superlattices," *Phys. Rev. Lett.* **58**(23), 2486–2489 (1987).
3. M. Soljacić and J. D. Joannopoulos, "Enhancement of nonlinear effects using photonic crystals," *Nat. Mater.* **3**(4), 211–219 (2004).
4. T. Baba, "Slow light in photonic crystals," *Nat. Photonics* **2**(8), 465–473 (2008).
5. M. Roussey, M.-P. Bernal, N. Courjal, D. Van Labeke, F. I. Baida, and R. Salut, "Electro-optic effect exaltation on lithium niobate photonic crystals due to slow photons," *Appl. Phys. Lett.* **89**(24), 241110 (2006).
6. B. Li, J. Zhou, L. Li, X. J. Wang, X. H. Liu, and J. Zi, "Ferroelectric inverse opals with electrically tunable photonic band gap," *Appl. Phys. Lett.* **83**(23), 4704 (2003).
7. W. Park and J.-B. Lee, "Mechanically tunable photonic crystal structure," *Appl. Phys. Lett.* **85**(21), 4845 (2004).
8. H. M. H. Chong and R. M. De La Rue, "Tuning of photonic crystal waveguide microcavity by thermo-optic effect," *IEEE Photon. Technol. Lett.* **16**(6), 1528–1530 (2004).
9. M. T. Tinker and J.-B. Lee, "Thermo-optic photonic crystal light modulator," *Appl. Phys. Lett.* **86**(22), 221111 (2005).
10. H. Lu, B. Sadani, N. Courjal, G. Ulliac, N. Smith, V. Stenger, M. Collet, F. I. Baida, and M.-P. Bernal, "Enhanced electro-optical lithium niobate photonic crystal wire waveguide on a smart-cut thin film," *Opt. Express* **20**(3), 2974–2981 (2012).
11. N. Courjal, S. Benhabane, J. Dahdah, G. Ulliac, Y. Gruson, and V. Laude, "Acousto-optically tunable lithium niobate photonic crystal," *Appl. Phys. Lett.* **96**(13), 131103 (2010).
12. G. Shambat, B. Ellis, M. A. Mayer, A. Majumdar, E. E. Haller, and J. Vučković, "Ultra-low power fiber-coupled gallium arsenide photonic crystal cavity electro-optic modulator," *Opt. Express* **19**(8), 7530–7536 (2011).
13. B. Schmidt, Q. Xu, J. Shakya, S. Manipatruni, and M. Lipson, "Compact electro-optic modulator on silicon-on-insulator substrates using cavities with ultra-small modal volumes," *Opt. Express* **15**(6), 3140–3148 (2007).
14. N. Courjal, B. Guichardaz, G. Ulliac, J.-Y. Rauch, B. Sadani, H. Lu, and M.-P. Bernal, "High aspect ratio lithium niobate ridge waveguides fabricated by optical grade dicing," *J. Phys. D Appl. Phys.* **44**(30), 305101 (2011).
15. T. Nishikawa, A. Ozawa, Y. Nishida, M. Asobe, F.-L. Hong, and T. W. Hänsch, "Efficient 494 mW sum-frequency generation of sodium resonance radiation at 589 nm by using a periodically poled Zn:LiNbO₃ ridge waveguide," *Opt. Express* **17**(20), 17792–17800 (2009).
16. M. Roussey, M.-P. Bernal, and F. I. Baida, "Experimental and theoretical observations of the slow-light effect on a tunable photonic crystal," *J. Opt. Soc. Am. B* **24**(6), 1416–1422 (2007).

17. M. Paturzo, D. Alfieri, S. Grilli, P. Ferraro, P. De Natale, M. de Angelis, S. De Nicola, A. Finizio, and G. Pierattini, "Investigation of electric internal field in congruent LiNbO₃ by electro-optic effect," *Appl. Phys. Lett.* **85**(23), 2875 (2004).
18. M. de Angelis, S. De Nicola, A. Finizio, G. Pierattini, P. Ferraro, S. Grilli, M. Paturzo, L. Sansone, D. Alfieri, and P. De Natale, "Two-dimensional mapping of electro-optic phase retardation in lithium niobate crystals by digital holography," *Opt. Lett.* **30**(13), 1671–1673 (2005).
19. M. Paturzo, P. Ferraro, S. Grilli, D. Alfieri, P. De Natale, M. de Angelis, A. Finizio, S. De Nicola, G. Pierattini, F. Caccavale, D. Callejo, and A. Morbiato, "On the origin of internal field in Lithium Niobate crystals directly observed by digital holography," *Opt. Express* **13**(14), 5416–5423 (2005).
20. G. W. Burr, S. Diziain, and M.-P. Bernal, "The impact of finite-depth cylindrical and conical holes in lithium niobate photonic crystals," *Opt. Express* **16**(9), 6302–6316 (2008).
21. M. Levy, R. M. Osgood, R. Liu, L. E. Cross, G. S. Cargill III, A. Kumar, and H. Bakhr, "Fabrication of single-crystal lithium niobate films by crystal ion slicing," *Appl. Phys. Lett.* **73**(16), 2293 (1998).
22. D. Djukic, G. Cerda-Pons, R. M. Roth, R. M. Osgood, Jr., S. Bakhr, and H. Bakhr, "Electro-optically tunable second-harmonic generation gratings in ion-exfoliated thin films of periodically poled lithium niobate," *Appl. Phys. Lett.* **90**(17), 171116 (2007).
23. G. Poberaj, M. Koechlin, F. Sulser, A. Guarino, J. Hajfler, and P. Günter, "Ion-sliced lithium niobate thin films for active photonic devices," *Opt. Mater.* **31**(7), 1054–1058 (2009).
24. F. Sulser, G. Poberaj, M. Koechlin, and P. Günter, "Photonic crystal structures in ion-sliced lithium niobate thin films," *Opt. Express* **17**(22), 20291–20300 (2009).
25. R. Geiss, S. Diziain, R. Iliew, C. Etrich, H. Hartung, N. Janunts, F. Schrepel, F. Lederer, T. Pertsch, and E.-B. Kley, "Light propagation in a free-standing lithium niobate photonic crystal waveguide," *Appl. Phys. Lett.* **97**(13), 131109 (2010).

1. Introduction

During the last 3 decades, there has been a great interest in photonic crystals (PCs) due to their ability to manipulate photons and to their potential applications in ultra-compact photonic devices [1, 2]. By replacing standard optical devices by the equivalent PC optical devices, a considerable size reduction can be achieved [3, 4], leading to micro and nano-scale switches, modulators, etc. In the perspective of integrating dense optical circuits on small-scale, tunable PCs present special interest. They typically consist of a periodic lattice of air holes graved into a dielectric substrate in which the optical properties are modified alternatively by an external physical signal such as electric or magnetic field, temperature, strain, etc [5–11]. In the case of silicon and other semiconductor materials, tremendous progress in photonic crystal fabrication has been made. However, up to now, electro-optically tunable PCs in silicon have limited tunability and modulation because of their low free carrier dispersion coefficient [12, 13] which leads to small attainable changes in the refractive index.

In the purpose of obtaining complex integrated photonic device such as ultra-compact, high speed and low power consumptions switches, modulators, etc., lithium niobate (LN) is a perfect candidate. The choice of LN is motivated by its numerous multi-physical properties, such as electro-optic, acousto-optic, etc. In previous works, we have fabricated LN photonic crystals of square lattices and shown an experimental realization of a tunable photonic band gap (PBG) [5]. One additional step is achieved in this work towards the fabrication of a tunable, low-voltage and micrometric-sized electro-optic intensity modulator based on PC cavity.

In addition, we demonstrate that the electro-optic tunability of a PC Fabry-Perot (FP) cavity can be significantly enhanced if the device operates at the cavity mode. It is well known that nonlinear effects can be enhanced in slow light regime as a result of the compression of the local density of states [3]. Here, slow light is exploited to enhance the electro-optic tunability [5, 10] of a LN PC cavity, the enhancement is improved with respect to previous works [10] thanks to vertically deposited electrodes. Moreover, the active length of interaction is only of 6 μm with an efficient tunability of 0.6 nm/V and a relative low driving electrical power (10 dBm).

2. Device design

A schematic of the proposed FP cavity PC is depicted on Fig. 1. An Annealed Proton Exchange (APE) process is firstly done on the congruent LN substrate to obtain vertical light confinement. In the lateral direction, optical grade dicing [14, 15] is used to obtain a ridge waveguide of $17\ \mu\text{m}$ wide and $50\ \mu\text{m}$ deep containing the APE waveguide. Waveguiding is then achieved by injecting a TE-like mode on the end facet of the APE waveguide when an X-cut LN wafer and Y-propagation are chosen.

The PC structure (see Fig. 1) consists of a triangular lattice of air holes oriented along the ΓM direction. The FP configuration, one line of defect perpendicular to the light propagation direction, is composed of 5 rows of holes from each side of the defect line.

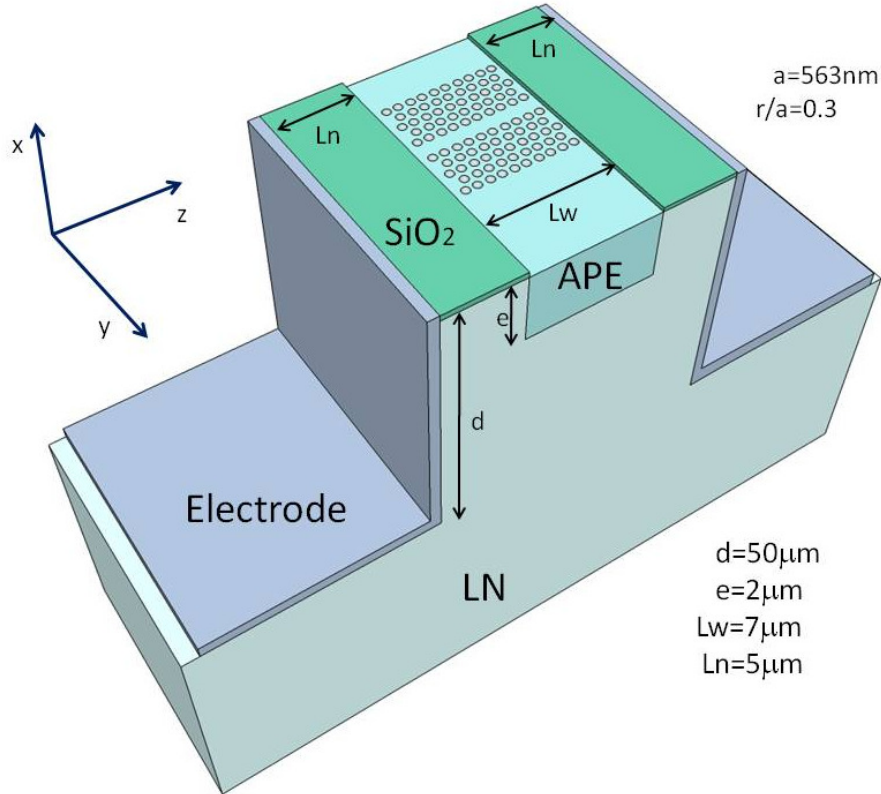


Fig. 1. Schematic of the PC F-P cavity modulator.

Plan Wave Expansion (PWE) with supercell technique simulations have been performed in order to obtain the dispersion diagram of the structure. A FP cavity mode corresponding to the flat band inside the PBG at $a/\lambda = 0.36$ of Fig. 2 is obtained for $r/a = 0.3$, r is the air hole radius and $a = 563\ \text{nm}$ is the hole periodicity. This last parameter is set so that the operating wavelength value is $\lambda = 1550\ \text{nm}$.

For this flat cavity mode where light slowly propagates, nonlinear effects could significantly be enhanced. In the present work we focus on the enhancement of the electro-optic effect. This enhancement can be quantified with the local field factor [10, 16].

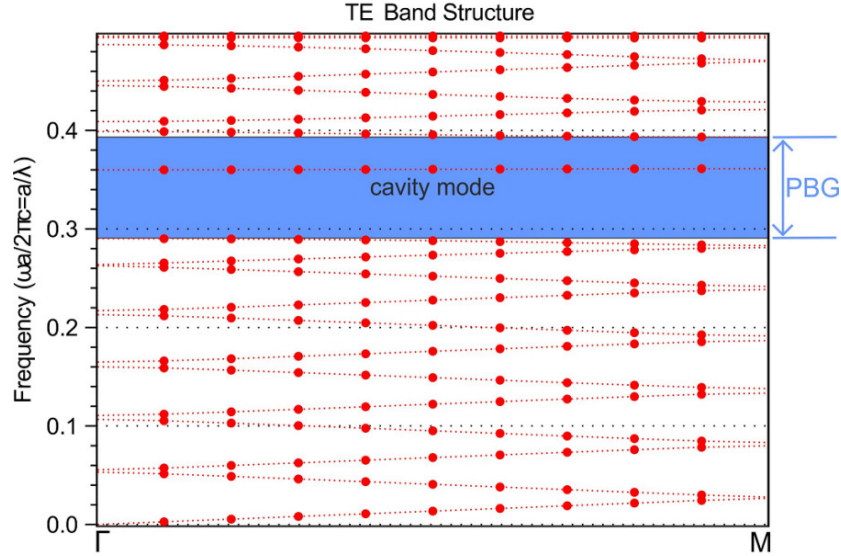


Fig. 2. Band structure of the PC FP cavity.

In fact, the index of refraction variation in LN is described by the Pockels effect and it is written as:

$$\Delta n = -\frac{1}{2} n^3 r_{33} f_{opt}^2 f_{el} \frac{V}{L} \quad (1)$$

Here, n is the index of refraction of LN, r_{33} is its electro-optic coefficient, f_{el} and f_{opt} are the local electrical and optical field factors respectively [17, 19], V is the applied voltage and L is the distance between the two electrodes. The factor $f_{opt} = 3.02$ is calculated as described in previous work [10]. The local electric field factor f_{el} is numerically estimated by finite element simulations. In our case, we use the commercial software Comsol with a configuration of vertically deposited electrodes which are placed parallel to the light propagation (see Fig. 1). For illustration, the electric field distribution with an applied external 10 V voltage is shown on Fig. 3. The real ridge structure with vertically deposited electrodes has been taken into account for simulations. The factor f_{el} is determined by the ratio of the electric field inside PC cavity structure (E_{PC}) over the electric field without PC cavity (E_B). In this case, f_{el} is around 2.25. This value is slightly higher than for planar electrodes. Consequently, the theoretical total enhancement factor ($f_{opt}^2 f_{el}$) of the electro-optic effect, which is in fact the overlap between optical field and electrical field, is of ~20.5. This value can be enhanced by increasing the number of the rows of air hole from each side of the defect line at the expense of transmission signal decrease. The current design, 5 rows in each side of cavity is a suitable compromise.

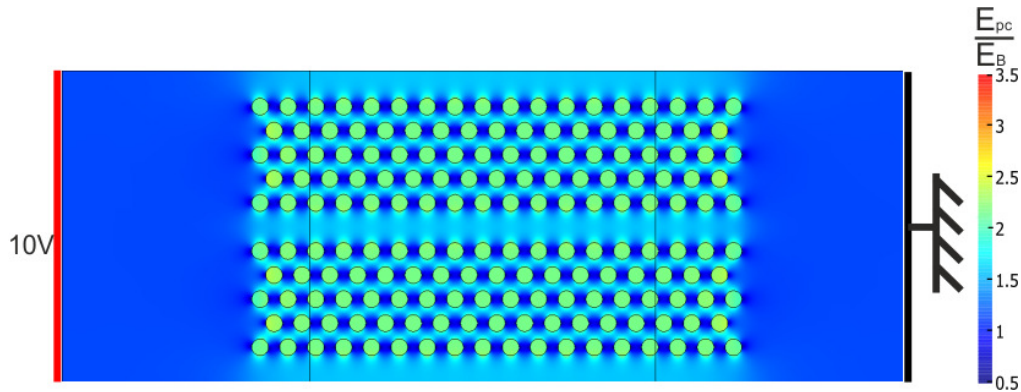


Fig. 3. Normalized static electric field distribution inside and around the LN PC FP cavity structure.

3. Fabrication

3.1. Hybrid waveguide

APE LN waveguide was fabricated on a 500 μm thick X-cut LN wafer, which is sandwiched by a ridge waveguide (see Fig. 1) as mentioned before. The different steps of the fabrication process are shown in Fig. 4. The first step consists of creating vertical light confinement. This is achieved by fabricating an APE waveguide through a SiO_2 mask (Fig. 4(a) and 4(b)). The proton exchange is performed with benzoic acid at 180°C for 2 hours which is followed by an annealing of the optical waveguide at 333°C for 6 hours. This produces a TE-polarized guided mode [5, 10, 16] centered at about 1.7 μm below the surface.

The second fabrication step is the fabrication of the ridge structure. A $\sim 2.5 \mu\text{m}$ thick layer of resist S1828 is homogeneously spread out on the sample (Fig. 4(c)) for protection purposes. An optical grade dicing machine with a circular precision saw (DISCO DAD 321) is used to create the ridge [14,15] (Fig. 4(d)).

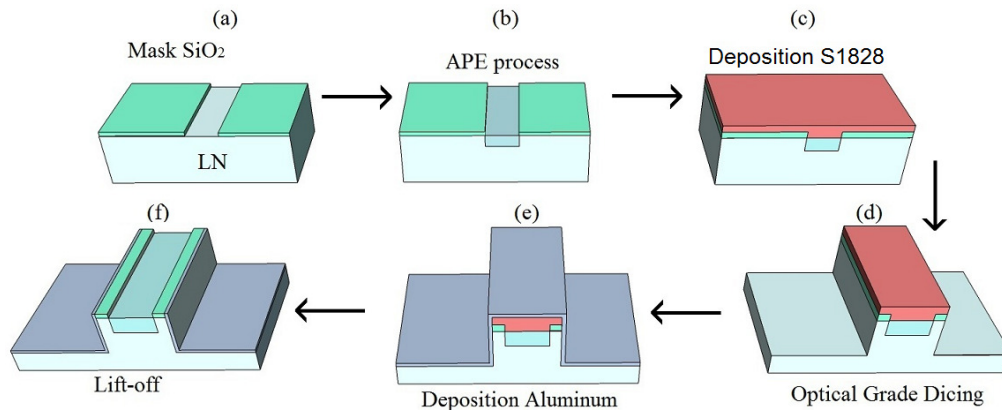


Fig. 4. Flow chart of the hybrid waveguide fabrication.

The next step consists of the electrodes fabrication on the vertical sidewalls of the ridge waveguide. This is done by depositing 200nm of aluminum by sputtering technique (Fig. 4(e)), followed by a lift-off process obtaining the electrodes between both sides of the waveguide region (Fig. 4(f)).

The top view of realization of the hybrid waveguide is shown in Fig. 5(a), the experimental guided mode visualized with an infrared camera (HAMAMATSU: C2741-03) and an Objective 40X at $\lambda = 1550 \text{ nm}$ can be seen in Fig. 5(b).

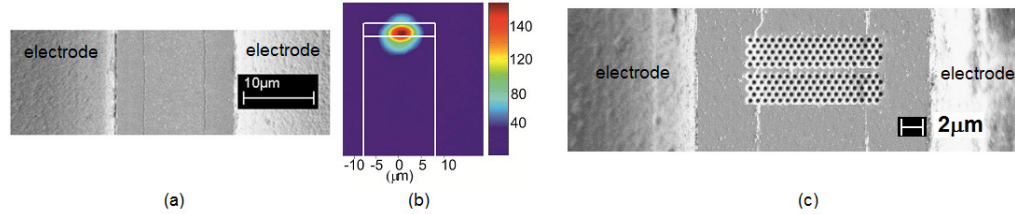


Fig. 5. (a) Top view SEM image of hybrid waveguide, (b) optical mode characterization of the waveguide where white lines denote the ridge waveguide and (c) top view SEM image of the fabricated PC FP cavity structure.

3.2. PC structure

The final step is to fabricate the PC on the hybrid waveguide. Holes are directly mechanically engraved by Focused Ion Beam (FIB) milling. Figure 5(c) shows a SEM image top view of the final structure.

4. Optical characterizations

4.1. Optical transmission

The optical transmission of the device is characterized using the experimental setup illustrated in Fig. 6 (blue dashed path). A supercontinuum source (LEUKOS SM-20) and an Optical Spectrum Analyzer (OSA from Anritsu MS9710A) are used. A polarization controller is adjusted for a TE-like polarization in the APE waveguide. Light is coupled into the waveguide using a Lensed Fiber (LF) with a focus spot size of $3 \mu\text{m}$. Similarly, the output of transmitted light is collected by another LF into the OSA. The normalized transmission spectrum (the transmission spectrum of the waveguide + PC normalized by the spectrum without the PC) through the PC cavity is shown in Fig. 7. The left photonic band edge located between 1320 nm and 1430 nm is outlined by the gray area. An extinction ratio of almost 15 dB is experimentally measured.

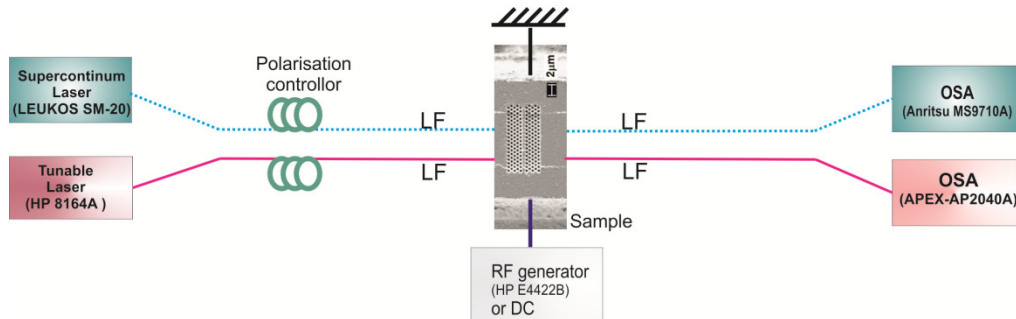


Fig. 6. Experimental setup for optical transmission (blue dashed path) as well as tunability and modulation performance (red solid path) characterizations. OSA indicates the optical spectrum analyzer and LF the lensed fiber.

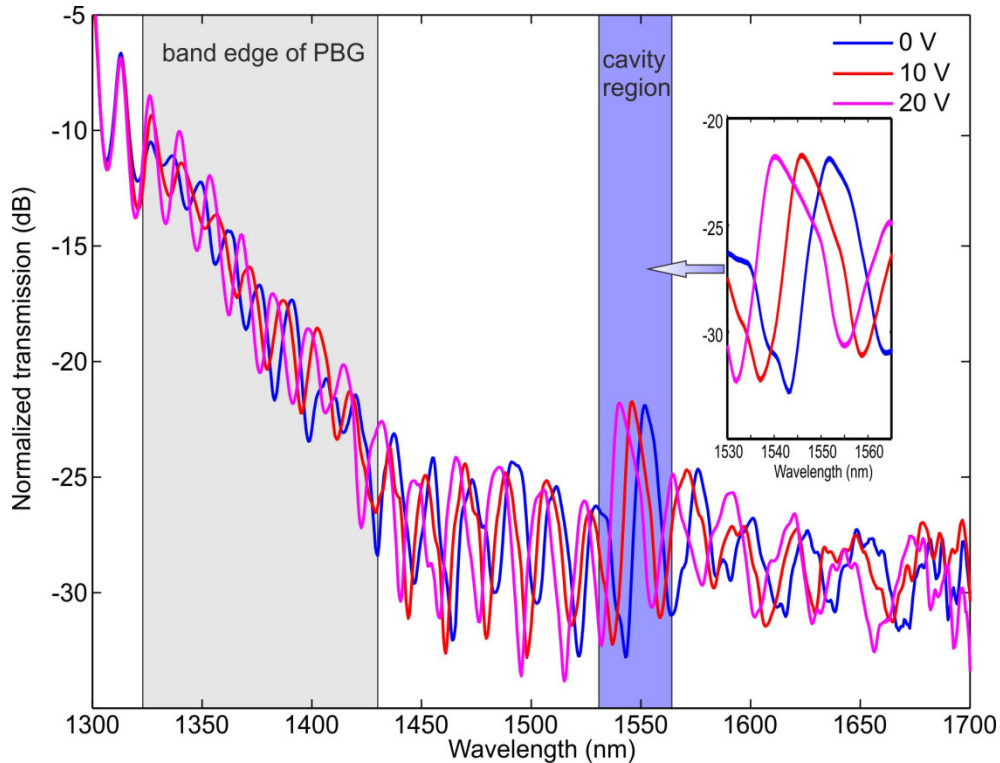


Fig. 7. Normalized transmission spectra of the PC cavity structure for three different applied voltage values (DC = 0 V, 10 V and 20 V) and the inset figure is the zoom of the cavity region.

The cavity peak resonance is located approximately at 1552 nm if no external signal is applied (DC = 0 V). It is less evident to see it than in the theoretical prediction because of the relatively large noise level and losses that can be attributed to the fabrication imperfections [5, 10, 16], as LN is a well known material for its resistivity to be etched [19].

Note that the oscillations in the transmission spectrum are explained by the Distributed Bragg Reflector (DBR) effect [13, 20] that takes place inside this PC FP cavity structure, especially for the APE waveguide since it processes a low contrast index of refraction.

4.2. Tunability

We have also tested the device performance tunability via the electro-optic effect. As it can be seen in the inset of Fig. 7, the FP cavity resonance is blueshifted when the applied voltage increases. We have measured this shift for different V as shown in Fig. 8(a), implying a tunability of ~ 0.6 nm/V, which is 18.3 fold larger than $r_{33} = 30.8$ pm/V. This experimental result is in good agreement with the theoretical predictions performed by FDTD that give a simulated tunability of ~ 0.7 nm/V.

To estimate the transmission dependence on the applied bias, we replaced the supercontinuum source by a tunable laser (HP 8164A) as shown in the red solid path of Fig. 6. The operating wavelength was 1546 nm (located in the raising edge of the cavity peak resonance). A high resolution OSA (APEX – AP2040A) with an optical resolution of 0.16 pm (20MHz) was utilized to determine the transmission intensity. Figure 8(b) presents the normalized intensity variations as a function of the applied voltage. A maximum of 11 dB variation can be achieved for an applied voltage varying from ~ 4 V to ~ 8 V.

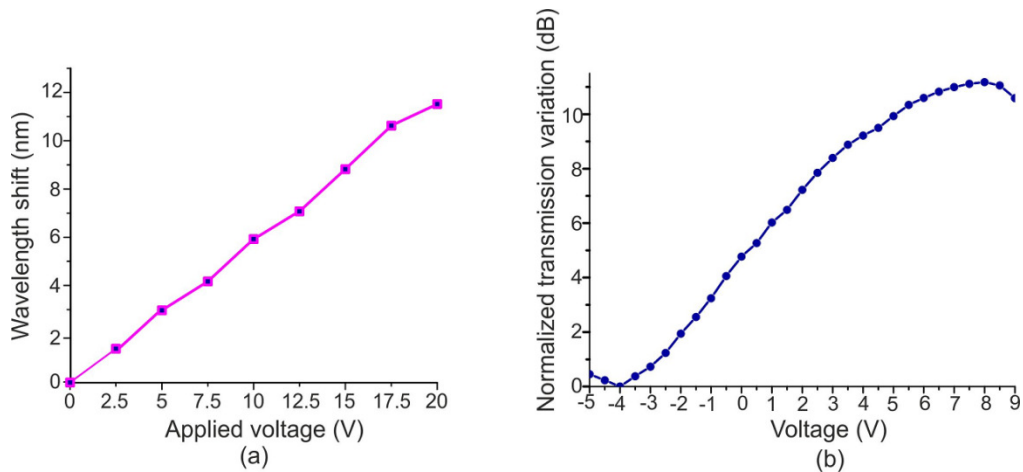


Fig. 8. Tunable performance of the device (a) wavelength shift as a function of applied voltage (b) transmission as a function of applied DC for a wavelength of 1546nm.

4.3. Modulation performance

The Intensity Modulation Frequency Response (IMFR) of the device has also been experimentally investigated. As shown in Fig. 6 (red solid path), the output LF was coupled to the OSA (Band C - AP2040A). In addition, a radiofrequency (RF) generator (HP E4422B) was connected to the electrodes. To ensure a correct separation of the sidebands modulation, the modulation frequency started from 50 MHz as the resolution of the OSA is 20MHz. Figure 9 shows the output power difference between the sidebands modulation signal and the laser ($\lambda = 1546\text{nm}$) through the entire device as the modulation frequency increases from 50MHz to 2 GHz. To do that, the driving electrical power of the RF generator was fixed to 10 dBm which warrants the modulation performance operating in relative low signal regime. Note that a compromise was found among the low driving voltage, the ratio of modulation and the distortion of modulated signal. The global frequency response corresponds to a low-pass filter which was expected since we had not optimized the electrodes for 50 Ohm matching, and that creates the capacitive effect which limits the bandwidth of the device. We see in inset 1 of Fig. 9, at the relative low frequency (160 MHz), the presence of the harmonic generations but their intensities are significantly lower by 20 dB than the sidebands modulation signal.

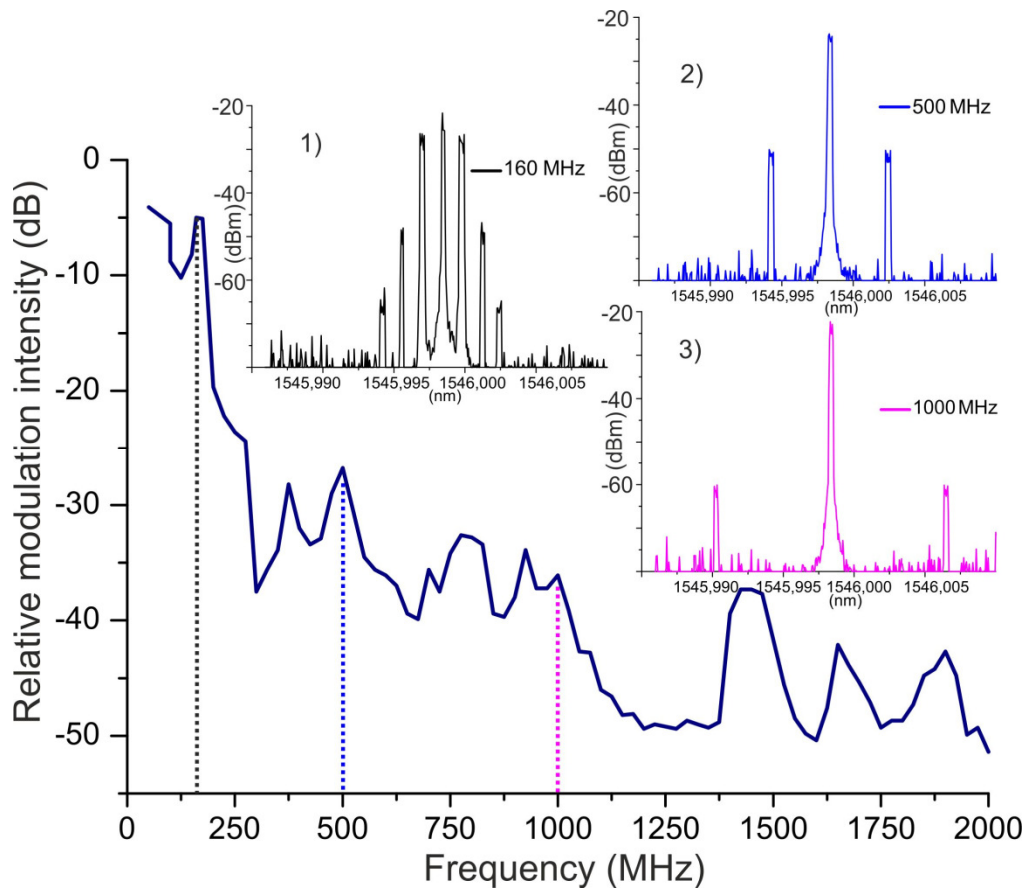


Fig. 9. Difference between the output powers of the sidebands modulation signal and the laser (1546 nm) for electro-optical modulation response through the entire device. The inset figures illustrate the electro-optical response showing the output powers of the laser (1546 nm) and the modulated sidebands signal at 1)160 MHz, 2)500 MHz, and 3)1000 MHz, respectively.

5. Discussion

From the results found in this paper, several improvements can be made especially in the holes fabrication. In fact, the APE waveguide center mode is at $1.7 \mu\text{m}$ from the surface while the FIB milling at this depth produces conical shape holes due to material redeposition. Thus, the device optical performances (losses, amplitude of resonant cavity peak, etc.) are degraded [5, 20]. This could be bypassed by using thin LN films or air suspended membranes [20–25].

Another improvement on the electro-optic performance can be made by decreasing the distance between the two electrodes. Currently, this distance is of $17 \mu\text{m}$ and is determined by the optical grade dicing resolution. Shorter distances between the 2 electrodes (for example $\sim 8.5 \mu\text{m}$) will double the electro-optic effect. This can be done easier with a dicing machine that provides better cutting precision.

In addition, the electrodes are not 50 Ohm impedance matched. This limits the modulation performance when the frequency grows up to the GHz range. More suitable electrode design should easily overcome these limits and reach ultra-high speed modulation.

6. Conclusion

In summary, we have theoretically and experimentally demonstrated the feasibility of a compact electro-optic modulator on a LN PC cavity structure with an active length of only 6

μm by combining the slow light effect with vertical formed electrodes. This novel configuration shows a tunability of 0.6nm/V , and the relative low driving electrical power (10dBm) modulation has been characterized. By optimizing both the optical confinement of high quality factor PC cavity and the electric performance (approaching the electrodes and matching the impedance), we believe that more compact and low energy consuming modulators operating in the GHz range may be realized.

Acknowledgment

This work has been carried out within project (PhoxCry) No. ANR-09-NANO-004 funded by ANR (P3N2009) France. The authors would like to thank B. Guichardaz and V. Petrini for helpful support in clean room. Huihui Lu is also financially supported by the Conseil Régional de Franche-Comté, France.